Holographic PIV System Using a Bacteriorhodopsin (BR) Film

Thomas Ooms[1], Victor Chan[1], Jerry Westerweel[1], Wouter Koek[2], Nandini Bhattacharya[2], and Joseph Braat[2]

[1] Faculty of Mech. Engineering, Delft University of Technology, Delft, The Netherlands, t.a.ooms@wbmt.tudelft.nl
[2] Faculty of Applied Sciences, Delft University of Technology, Delft, The Netherlands

Abstract. We present a holographic particle image velocimetry system that uses a reusable holographic material as the recording medium. The measurement system records double-exposure holograms in a film containing the photochromic protein bacteriorhodopsin (BR). The two constituent particle holograms are recorded in a single film using polarization multiplexing. We describe the system in detail and present three-dimensional measurements that determine the system's accuracy and demonstrate its capabilities.

1 Introduction

Particle image velocimetry (PIV) is a common and valuable technique for the study of fluid flows [1]. In its basic form PIV yields planar two-component flow-field information. Although special stereoscopic or scanning implementations have been developed [2, 3], it has been impossible to perform truly instantaneous three-dimensional three-component flow measurements with these PIV methods.

The need for instantaneous three-dimensional three-component flow measurements for both engineering and fundamental flow studies suggests the use of holographic imaging systems, and much effort is currently focused on the development of such systems. Although several successful holographic particle image velocimetry (HPIV) systems have been demonstrated, they all use silver-halide film as the holographic medium [4–7]. The chemical development associated with such films introduces distortion to the recorded hologram, requires a skilled person for the development, and is time consuming. Digital HPIV forms an alternative to film-based HPIV [8]. However, the space-bandwidth of current state-of-the-art CCDs is very small when compared to holographic film, thereby limiting the number of flow vectors that can be obtained from one recording. *Barnhart* et al. [9] realized that a practical HPIV system must use a holographic film that does not require development, and they suggested the use of bacteriorhodopsin (BR).

In this chapter we present the first operational HPIV system to employ BR as the recording material. Furthermore, the presented HPIV system is the

A. Schroeder, C. E. Willert (Eds.): Particle Image Velocimetry,
Topics Appl. Physics **112**, 171–189 (2008)

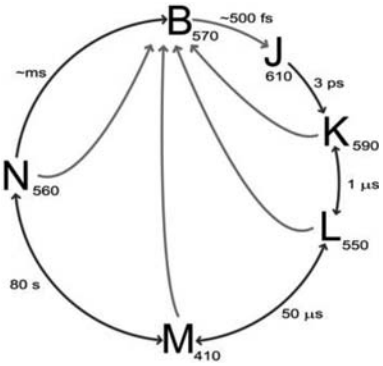

Fig. 1. Photocycle for D96N BR. *Black arrows* indicate a thermal transition. *Gray arrows* indicate photoinduced transitions. The absorption peak for each photointermediate is shown

first to use polarization multiplexing for the independent recording of the two particle holograms. We will show results to demonstrate the system's capabilities for the study of three-dimensional three-component flow fields.

2 BR Films

In nature, the photochromic protein BR plays a crucial role in the photosynthetic system of the salt-marsh bacterium Halobacterium salinarium [10]. BRs are found in the bacterial cell membrane in the form of two-dimensional crystalline patches. These patches have a diameter of up to 5 µm and are called purple membrane (PM). Upon absorption of light the BR molecule transports a proton from the cell's cytoplasm to the outer medium. The energy that is stored in this proton gradient is used by a membrane-bound enzyme (ATPase) to regenerate adenosine triphosphate (ATP) from adenosine diphosphate (ADP). Like all other living cells, the halobacterium uses ATP as the energy source to drive its cellular molecular processes. Effectively, the bacterium uses BR to convert sunlight directly into chemical energy.

Prior to absorption of a photon the BR molecule is in the ground state, called B. The absorption of a photon triggers a sequence of molecular configurational changes resulting in the pumping of a proton, and finally leading the molecule back into the B state. Due to their different molecular configurations the various intermediates exhibit different absorption spectra.

Figure 1 displays the photocycle of BR, and shows the absorption maxima of the various intermediates. As shown in Fig. 2, the BR photocycle is often simplified by adopting a two-state model using B and M. Not only is M the longest-lived intermediate state, its shift of the absorption peak over 160 nm is much greater than that of any other state. The ability to use light to induce a large modulation of the optical density makes the protein a good

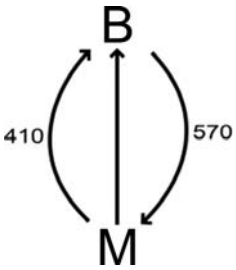

Fig. 2. Simplified two-state model of the BR photocycle

material for optical recording. Since the configurational changes also lead to a change in refractive index of the order of 10^{-3}, BR can be used for combined phase-amplitude recordings. The protein's size, that is of the order of a few nanometers, combined with the dense packing of BR within PM, allows for high-resolution recording ($> 5000\,\mathrm{lp/mm}$). The above-mentioned features make BR very attractive as a reversible holographic recording medium, and as such BR has been integrated in an interferometric measurement system [11].

When illuminating the protein with linearly polarized light, for the probability P to initiate a photoinduced transition can be written:

$$P(\varphi) \propto \cos^2 \varphi + k_1 \sin^2 \varphi\,, \tag{1}$$

where φ is the angle between the molecule's long axis and the plane of polarization of the exciting light, and the dichroic ratio $k_1 = 0.04$. Illuminating a normally isotropic collection of BR molecules with linearly polarized light will thus result in a photoinduced anisotropic distribution of molecules in the B and the M state. *Kakichashvili* [12] was the first to realize the extra possibilities that materials with photoinduced anisotropy offer for holographic recording. He showed the feasibility of recording a hologram in polarization-sensitive materials using an object and reference wave with orthogonal polarizations, both linear and circular, by recording a varying state of polarization rather than recording a varying state of intensity, as is done in traditional holography.

Through many millions of years of evolution BR has been optimized for light absorption and energy conversion. Unfortunately, the requirements for an intracellular energy converter tend to differ from those for a holographic recording material. For example, in wild-type (WT) BR, the form as it is found in nature, the half-lifetime of the M state is only 15 ms. This rapid loss of information makes the medium too volatile for many practical applications. However, several genetic variants exist that have different properties from WT BR. The mutant used in our experiments is D96N. Obtained through random mutagenesis this variant has an M half-lifetime of 100 s, thereby providing more time to extract the information contained in a hologram.

Table 1. The polarization of the reconstructed image is shown for different combinations of the reference beam, object beam, and reconstruction beam polarization (L = LHCP, R = RHCP, – indicates no image is reconstructed)

Reference beam	Object beam	Reconstruction beam	Reconstructed image
L	R	L	R
L	R	R	–
R	L	L	–
R	L	R	L

For use in a technical application it is practical when the BR is contained in a film. Fortunately, upon extraction of PM from the bacterial cell the protein BR maintains its functionality. The extracted PM can be embedded in a film matrix that is subsequently sandwiched between two glass plates. The obtained film has a homogeneous optical density and a uniform thickness. Since the angular distribution of BR is isotropic, the film is well suited for the recording of polarization holograms. The film used in this experiment has an aperture of $100 \times 100\,\text{mm}$, a thickness of $30\,\mu\text{m}$, and optical density of 1.5 at 570 nm, and is commercially available from Munich Innovative Biomaterials (MIB) GmbH.

3 Polarization Multiplexing

Polarization holograms have the unique ability to modify the polarization of the reconstruction beam resulting in a reconstruction of the original object polarization. Polarization holograms formed by two orthogonal circularly polarized waves also have the ability of reconstructing an image in the $+1$ order only and not in the -1 order and *vice versa* [13]. *Koek* et al. demonstrated the crosstalk-free polarization multiplexing of two images in BR, using either a sequential or a simultaneous reconstruction [14, 15]. As is illustrated in Table 1, the technique of sequential readout polarization multiplexing involves recording the first image using left-hand circular polarization (LHCP) for the reference beam, and right-hand circular polarization (RHCP) for the object beam.

The second image is then recorded using RHCP for the reference beam and LHCP for the object beam. If the hologram is reconstructed with LHCP the first recorded image will be reconstructed having RHCP, whereas the second image is fully suppressed. Alternatively, if the hologram is reconstructed using RHCP the second image is reconstructed having LHCP, while the first image remains absent. Thus, by choosing the proper polarization for the reconstruction beam the two holographically stored images can be retrieved independently. This is the type of multiplexing that is used for the experiments presented in this chapter.

The ability to use polarization multiplexing gives polarization-sensitive materials (such as BR) a distinct advantage for use in HPIV over nonpolarization sensitive materials (such as silver halide, or photopolymer films). HPIV systems based on silver-halide films normally use angular multiplexing to store the two constituent holograms. The need for two reference beam paths obviously makes the system more complex and subject to alignment errors. Polarization multiplexing allows both pulses to follow a common beam path, thereby keeping the system simple.

4 Holographic Imaging System and Data Processing

The potential of our holographic imaging system is investigated by performing three experiments; a calibration measurement, a jet-flow measurement and a vortex-ring flow measurement. The first two experiments (calibration and jet flow) are performed with a similar imaging system configuration and a similar data-processing method. These are described in Sect. 4.1. The third experiment (vortex-ring flow) is performed with an improved imaging system and an improved data-processing method, as described in Sect. 4.2.

4.1 System Configuration of Calibration Measurement and Jet-Flow Measurement

Our HPIV system based on polarization multiplexing in BR will be demonstrated by means of experiments on a water jet seeded with 100 μm solid glass spheres. As is illustrated in Fig. 3 the jet is injected into a tank of clear water through a syringe nozzle having an exit diameter of 2 mm. With a tank width of 50 mm the wall boundaries should have little influence on the near field of the flow.

In contrast to the neutrally buoyant hollow glass spheres that are frequently used in PIV, the solid glass spheres used in this experiment are obviously heavier than water, thereby influencing the fluid flow. However, the choice of particle ensures maximum efficiency of the object illumination beam. Rather than scattering in all directions as is the case with hollow glass spheres, a solid glass sphere acts as a ball lens directing almost all the incident light into a more or less uniform cone with NA = 0.15. This value of the NA was determined by performing a three-dimensional scan of the holographic reconstruction of such a particle.

In the remainder of this section we will discuss the three main steps that are involved in performing a holographic measurement; recording a hologram, reconstructing the hologram, and finally analyzing the data. In the next section we will present the experimental results.

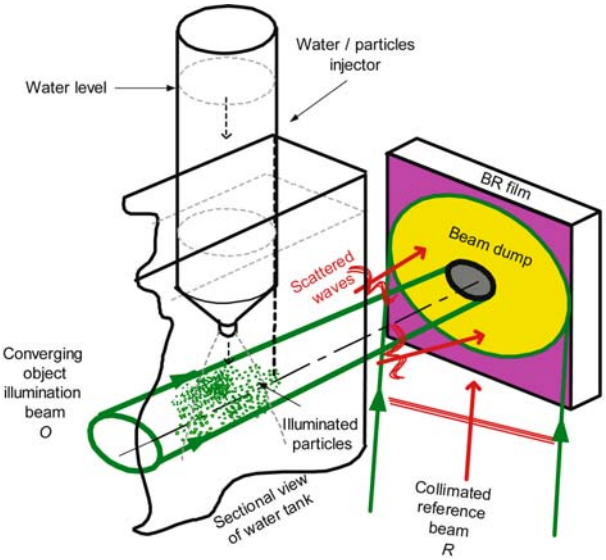

Fig. 3. Schematic drawing of analyzing jet flow by holographically recording the particle field in BR

4.1.1 Recording the Hologram

In order to detect the velocity of the particles, their location must be recorded twice with a known time separation between the two recordings. By means of polarization multiplexing the spatial distribution of the particle field at the two moments is recorded into a single BR film using the experimental setup shown in Figs. 3 and 4. Prior to each recording the BR film is exposed to light from a UV LED array (410 nm). This erases any prior information in the film by forcing all molecules into the B state (Fig. 2). The holograms are recorded using a pulsed frequency-doubled Nd:YAG laser that outputs a maximum of 320 mJ per 7 ns pulse at 532 nm into a beam with 8 mm beam diameter. Using a half-wave plate and a Glan laser polarizer the light from the pulsed Nd:YAG laser is split into an object illumination wave O, and a reference wave R. The quarter-wave plates are adjusted such that when the Pockels cells are inactive the reference beam has LHCP at the location of the BR film, and the object beam has RHCP at the location of the BR film. Upon activation, the Pockels cells function as half-wave plates allowing to record the second hologram using RHCP for the reference beam and LHCP for the object beam. After passing through the Pockels cell wavefront R is expanded to 65 mm and collimated by lenses L1 and L2, after which it falls onto the BR film at an incidence angle of approximately 40°. Using lenses L3 and L4 wavefront O is expanded to 17 mm and made slightly convergent (NA = 0.005).

The convergent object illumination beam enters the tank of clear water, in which the injected particles close to the injection nozzle will refract the

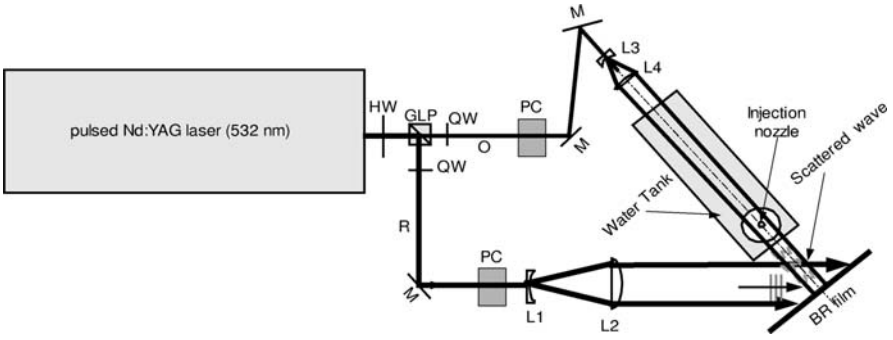

Fig. 4. Schematic for recording a double-exposed particle hologram. HW: $\lambda/2$ plate; GLP: Glan laser polarizer; QW: quarter-wave plate; O: object wavefront; R: reference wavefront; M: mirror; PC: Pockels cell; Lx: lens

incident light. The resulting divergent waves have NA = 0.15 inside the water tank and NA = 0.20 after exiting the tank. The NA of the holographic imaging system is sufficient to capture all the refracted light. The BR film is partially covered with a circular metallic film beam dump (diameter = 8 mm) to protect it from permanent damage by the unrefracted part of the object illumination beam. The beam dump also prevents the presence of the unrefracted beam in the reconstruction that leads to a better particle detectability. The refracted part of the light will fall onto the BR film and interfere with the reference beam to form a holographic recording of the particle field. At the location of the BR film wavefront R has a fluence of 5 mJ/cm^2. Wavefront O has a fluence of 80 mJ/cm^2 at the location of the injection nozzle, obviously only a fraction of this energy will contribute to the formation of the hologram. The system is controlled by dedicated timing electronics that synchronize the firing of the two laser cavities and the switching of the polarization between the two recordings.

Because the object beam is convergent, the beam dump on the BR film can be smaller than the cross-sectional area of the illuminated particle field. With this configuration more refracted light is captured on the holographic film than with a collimated object beam (which would require a beam dump that is as large as the cross-sectional area of the illuminated object). Because more scattered light is recorded on the film, more light is diffracted during reconstruction that leads to a higher reconstructed particle image intensity. Another elegant solution for this problem is using a hybrid geometry where the zeroth-order beam is filtered out by means of a Fourier filter [16]. This geometry is applied in the experiment of the measurement of the vortex ring (Sect. 4.2.1).

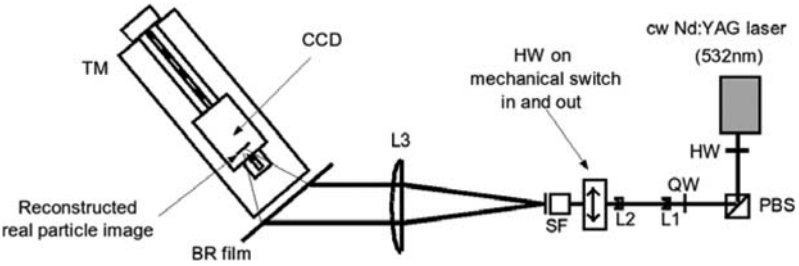

Fig. 5. Schematic for sequentially reconstructing two polarization multiplexed particle holograms. HW: $\lambda/2$ plate; PBS: polarizing beam splitter; QW: quarter-wave plate; Lx: lens; SF: spatial filter; TM: motorized translation mechanism

4.1.2 Reconstructing the Hologram

After the two particle holograms have been recorded, the information contained in the BR film must be extracted. This is done using the experimental setup in Fig. 5. Light from a CW frequency-doubled Nd:YAG laser (532 nm) is used for the reconstruction. Using a half-wave plate and polarizing beamsplitter the beam intensity can be adjusted. A quarter-wave plate converts the linearly polarized light to RHCP. By means of a half-wave plate that is mounted on a mechanical switch the beam can switch between RHCP and LHCP with speeds up to 10 Hz. This switching is used to alternate between the polarization multiplexed images. Lenses L1 and L2 expand the beam to fit the aperture of the spatial filter. Using the spatial filter and lens L3 the beam is expanded and collimated. At the location of the BR film the reconstruction beam has 65 mm diameter and an intensity of $130\,\mu W/cm^2$.

The reconstruction beam illuminates the BR film in a phase-conjugate manner. The holographic grating inside the BR film will diffract light to form real images of the recorded particle fields. A CCD camera (1376×1040 pixels, pixel size $6.45\,\mu m$) that is mounted on a motorized translation stage is used to digitize the three-dimensional intensity distribution. The three-dimensional field is digitized as 100 parallel planes. The frame capturing of the CCD camera, the motion of the translation stage, and the mechanical movement of the half-wave plate have been synchronized. As a result, each captured odd frame contains the intensity distribution of the first recorded particle field, whereas each captured even frame contains information concerning the second recorded particle field. This leads to 200 digitized frames per hologram. Currently, the various operations during reconstruction lead to a readout rate of about 2 frames per second, which leads to a total readout time of about 100 s. The translation mechanism moves the camera $25\,\mu m$ in between each frame. Therefore, the z-resolution for each particle field is currently $50\,\mu m$ in air. Because the particle field is recorded in water and reconstructed in air a longitudinal magnification is introduced during the reconstruction. This is illustrated in Fig. 6.

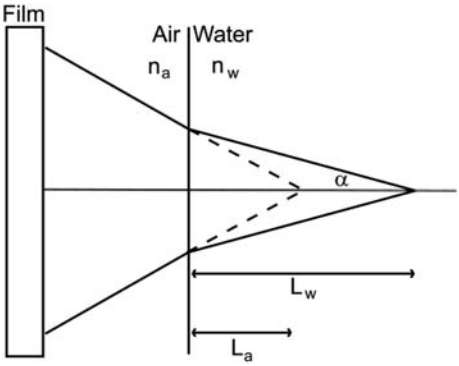

Fig. 6. Longitudinal magnification due to change in refractive index. *Solid lines* indicate the ray path during the recording (particle in water, BR film in air). The *dashed line* represents the ray path when during the reconstruction the air/water interface has disappeared

A particle is located at a distance L_w behind the air/water interface. Rays that come from the particle at an angle α with respect to the optical axis refract at the air/water interface and are recorded in the BR film. During the reconstruction, the light does not refract and the rays focus at a distance L_a behind the location where the air/water interface was at the time of recording. The distance that was traveled through water at the time of the recording is thus magnified by a factor $M = L_a/L_w$. It is easily shown that this magnification may be written:

$$M = \frac{n_a \sqrt{1 - \left(\frac{n_w}{n_a} \sin \alpha\right)^2}}{n_w \cos \alpha}, \tag{2}$$

where n_a and n_w are the refractive index in air (1) and water (1.33), respectively. For the particles that are used in this experiment (NA = 0.15) we find for the outer rays that M = 0.745. The dependency of the longitudinal magnification on the NA implies that the image will be affected by spherical aberration. Using ray tracing it can be shown that a point-source-like particle that is 20 mm into the tank and refracts light with NA = 0.15, will be reconstructed in air having a geometrical spot size of 16 μm. We did not take measures to minimize the induced spherical aberration. However, measurements that have higher NA, require a better z-resolution, or require higher particle-seeding densities, elimination of spherical aberration may be necessary. This can be achieved by introducing an equal amount of water between the BR film and the CCD camera during the reconstruction as was present between the particle of interest and the BR film during the recording. A ray-tracing program has shown that the spherical aberrations that are caused by refraction from the air/water interfaces can be completely eliminated with

this approach. Practically, this approach can be realized by placing an expandable water tank between the hologram and the CCD camera during reconstruction, with a fixed glass window on one side and a glass window on the other side of the tank that moves synchronized with the camera. (The tank would resemble an accordion musical instrument.) This approach removes the need to place the CCD chip inside a water-filled tank during reconstruction to eliminate the spherical aberrations.

When reconstruction is performed *with* an expandable water tank, the discussed spherical aberrations are absent and the inplane resolution (x–y) is only determined by the pixel size. When reconstruction is performed *without* an expandable water tank, spherical aberrations lead to a transverse particle-image diameter of 16 μm. This implies a small reduction of the accuracy of the transverse particle-image position. This reduction, however, is acceptable in the current experiments. In both cases there is no transverse magnification.

Being limited by computer memory we could capture 280 frames per measurement. Therefore, our reconstruction volume is currently limited to $7.0 \times 9.2 \times 7.0\,\mathrm{mm}^3$ in air. Due to the volatile nature of BR there is a slight decrease in image intensity and contrast during the reconstruction. All images are written to the computer's hard disk for subsequent analysis.

4.1.3 Data Extraction

The two sets of three-dimensional intensity distributions are used to create two three-dimensional particle location maps. Image processing is performed on each image to enhance the detectability of the reconstructed particles. This is achieved by using a phase-preserving denoizing image-processing routine outlined by *Kovesi* [17]. Next, we perform particle detection by crosscorrelating each image with a 5×5 Gaussian particle mask. After this correlation the software detects the local maxima in the correlation plane, corresponding to the particle centers. These two-dimensional particle maps are stacked to form a volumetric map containing particle streaks. One such streak obviously corresponds to a particle coming in, and going out of, focus. Within each streak every slice is given a value based on the unfiltered and unprocessed intensity value of the corresponding particle image. We found that the maximum intensity value serves as a reliable indicator for the particle's longitudinal position (see Fig. 7).

After the two three-dimensional particle location maps are retrieved, the particle displacement is determined using a nearest-neighbor search routine operating on the two datasets. A particle from the first dataset is thus assumed to have moved to the nearest particle in the other dataset. Obviously this is only valid when the mean particle displacement is smaller than the mean distance between two adjacent particles. Finally, the displacement in the z-direction is compensated for the induced magnification using (2). All image processing and data extraction is performed on a personal computer

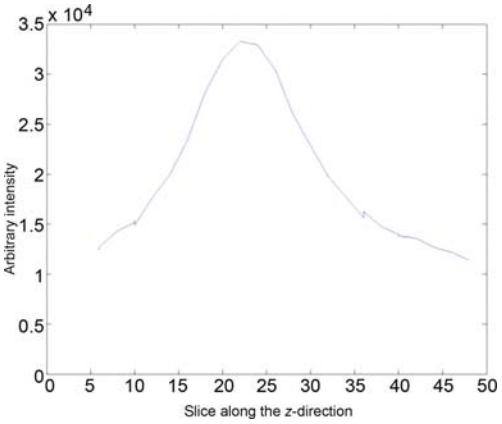

Fig. 7. Particle intensity as a function of position in reconstructed volume

using MATLAB. It typically takes 3–4 h to fully analyze 2 sets of 140 images, in total containing several hundreds of particles.

4.2 Configuration of Vortex-Ring-Flow Measurements

The configuration of the vortex-ring experiment is similar to the earlier described configuration, with the exception of some changes. The changes are described here.

4.2.1 Recording

As shown in Fig. 8, the object beam is expanded and collimated by lenses L3 and L4. The collimated object beam reaches a water-filled glass tank with a transverse beam-diameter of 32 mm and a typical fluence of 29 mJ/cm^2. The incoming light partially scatters from tracer particles and passes through a highpass optical Fourier filter that consists of a lens, L5, a beamstop and a lens, L6. L5 and L6 have a focal length, f, of 200 mm and a beamstop of 6 mm yields a Fourier filter spatial cutoff frequency of 28 mm^{-1}. The Fourier filter generates a real image (RI) of the tracer particles at distance f behind L6, which is recorded (380 mm further) on a BR film. The reference beam is expanded and collimated by lenses L1 and L2 and reaches the BR film with a fluence of 0.53 mJ/cm^2. The fluence values correspond to a beam-energy ratio between the object beam and the reference beam of 9 : 2 respectively. (Note: This ratio refers to the object beam fluence *before* it reaches the object. The scattered object light that passes the spatial Fourier filter and reaches the holographic film is significantly weaker.) These values are a result of experimental maximization of the reconstructed signal intensity.

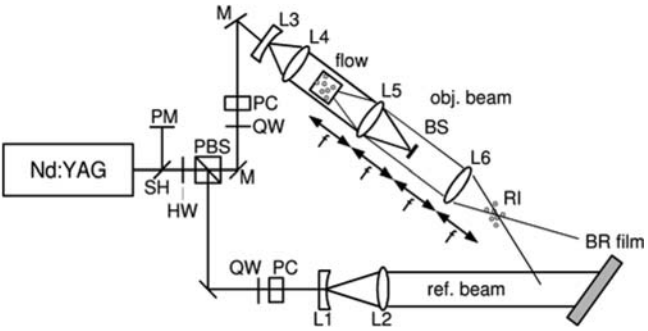

Fig. 8. Experimental configuration that is used for vortex-ring-flow measurements. BS: beamstop; RI: real image

The reference beam reaches the film at an angle of 26° from the film-normal, while the film-normal is positioned parallel to the optical axis of the object beam.

4.2.2 Flow

The flow around a vortex ring in water is measured. The tank size is increased to 60 mm (along the optical axis) ×135 mm (vertical) ×200 mm (horizontal, perpendicular to the optical axis). A tube filled with strongly diluted ink is placed just above the water surface (∼5 mm). Labview software controls the release of one droplet that forms a downward-traveling vortex ring. The double laser pulse is fired 1–2 s after the release of the droplet. The vortex ring is then in the illuminated part of the tank. The horizontal size of the vortex ring grows towards a typical size of 2 cm near the bottom of the tank.

The tracer particles in this experiment are hydrogen bubbles with a typical diameter of 20–30 μm. The hydrogen bubbles are generated by electrolysis of water. The typical traveling velocity of the vortex ring is five times larger than the maximum observed rise velocity of the hydrogen bubbles. This suggests that the hydrogen bubbles are reasonably suitable tracer particles in this experiment. Although the non-neutral buoyancy of the hydrogen bubbles is clearly a disadvantage, the strong scattering behavior makes their use attractive.

4.2.3 Reconstruction

The intensity of the reconstruction beam is, in the second experiment, $80\,\mathrm{mW/cm^2}$. This value is experimentally determined by considering two opposing effects: If the reconstruction-beam intensity is lower, the readout process becomes so slow that thermal-induced erasure of the hologram prevents successful readout of all frames. However, a higher reconstruction-beam

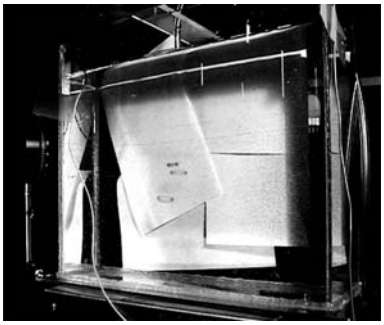

Fig. 9. Vortex rings are generated in a water-filled tank. For visualization, three vortex rings are generated in this photograph

intensity leads to excessive photoinduced erasure during overhead readout operations (i.e., stage motion, polarization switching).

4.2.4 Data Analysis

Data analysis is performed by MATLAB 7 on a conventional desktop computer (CPU: AMD 2.5 GHz, RAM: 1.8 GB, OS: Linux). Both reconstructions are each split into interrogation volumes. The size of an interrogation volume varies from 8 to 128 pixels in the transverse direction and is fixed at 8 pixels in the longitudinal direction. The volume overlap between adjacent interrogation volumes is generally 50 %. Interrogation volumes are processed comparably to conventional 2D digital PIV: a three-dimensional crosscorrelation is performed with an FFT algorithm according to this formula: the average intensity of the two interrogation volumes is subtracted and both volumes are zero-padded. A three-dimensional crosscorrelation is performed with an FFT algorithm: the FFT of interrogation volume 1 is multiplied by the complex conjugate of the FFT of interrogation volume 2. The absolute value of the inverse FFT of the product is calculated and the result then divided by the square root of the autocovariance of interrogation volumes 1 and 2 to obtain a 3D volume of crosscorrelation coefficients:

$$
\begin{aligned}
r_{12}(\boldsymbol{x}) &= \frac{\langle \tilde{I}_1(\boldsymbol{\xi}) \cdot \tilde{I}_2(\boldsymbol{\xi}+\boldsymbol{x}) \rangle}{\sqrt{\langle \tilde{I}_1(\boldsymbol{\xi}) \cdot \tilde{I}_1(\boldsymbol{\xi}) \rangle \cdot \langle \tilde{I}_2(\boldsymbol{\xi}) \cdot \tilde{I}_2(\boldsymbol{\xi}) \rangle}}\,, \\
&= \frac{\left| \mathrm{IFFT}\big(\mathrm{FFT}(\tilde{I}_1) \cdot \mathrm{FFT}^*(\tilde{I}_2)\big) \right|}{\sqrt{\langle \tilde{I}_1 \cdot \tilde{I}_1 \rangle \cdot \langle \tilde{I}_2 \cdot \tilde{I}_2 \rangle}}\,,
\end{aligned}
\tag{3}
$$

where $r_{12}(\boldsymbol{x})$ is the crosscorrelation coefficient, $\langle\,\rangle$ is the mean, $\tilde{I}_1$ and $\tilde{I}_2$ are the intensity data of interrogation volumes 1 and 2, respectively, after subtraction of the mean intensity and after zero-padding, $\boldsymbol{x}$ and $\boldsymbol{\xi}$ are three-dimensional spatial coordinates and * is the complex conjugate.

The integer-pixel position of the global maximum of the correlation cube $(x_{\text{peak}}, y_{\text{peak}}, z_{\text{peak}})$ is found and the correlation cube is then divided by a 3-dimensional kernel to compensate for the fact that each point in the correlation volume is the result of a different volume overlap between interrogation volume 1 and 2. Then, a subpixel estimate of the z-position of the correlation peak is determined by making a 7-point least-square Gaussian fit on the points between $(x_{\text{peak}}, y_{\text{peak}}, z_{\text{peak}} - 3)$ and $(x_{\text{peak}}, y_{\text{peak}}, z_{\text{peak}} + 3)$. No subpixel estimate is made of the x- and y-positions of the correlation peak because the accuracy of the integer-pixel position is currently sufficient.

5 Measurements

A series of measurements were performed using the described system. First, we calibrated the system's accuracy. Next, we used the holographic camera to analyze an actual flow.

5.1 Accuracy Test/Calibration

For testing the system's accuracy we prefer to induce a known physical shift to a particle field and verify the system's capability to retrieve the associated displacement vector based on two holographic recordings. For this purpose we obtained a tank with tracer particles in resin. Unfortunately, the resin depolarized the light, thereby introducing unwanted crosstalk into our polarization multiplexed holograms. An alternative approach was to stick particles onto a microscope slide, after which the microscope slide was mounted on a translation stage. However, we had practical problems in sticking the 100-μm glass particles to the microscope slide while maintaining a good optical quality. Based on before-mentioned experiences we decided to use an artificial or null shift rather than an induced physical shift of the particle field.

First, we recorded a hologram of the jet flow coming out of a syringe nozzle using one laser only. Using this single three-dimensional intensity distribution we created a second stack of images with an artificially induced known shift. The intensity of the second stack of images was altered to simulate a slight difference in diffraction efficiency between two actual reconstructed holograms. For multiple artificially induced shifts, in total having analyzed thousands of particle images, the software retrieved the actual displacement to within one pixel accuracy (x, $y = 6.45\,\mu\text{m}$, $z = 67\,\mu\text{m}$) for more than 95 % of the identified particles.

Next, we recorded a hologram of the jet flow coming out of a syringe nozzle using two orthogonally polarized laser pulses with a time separation of 10 μs. Given the speed of the jet this time delay was short enough such that only subpixel particle displacements should occur. Data extraction yielded 677 vectors, of which 647 were $[0, 0, 0]$. Again the system provided single-pixel accuracy for more than 95 % of the vectors.

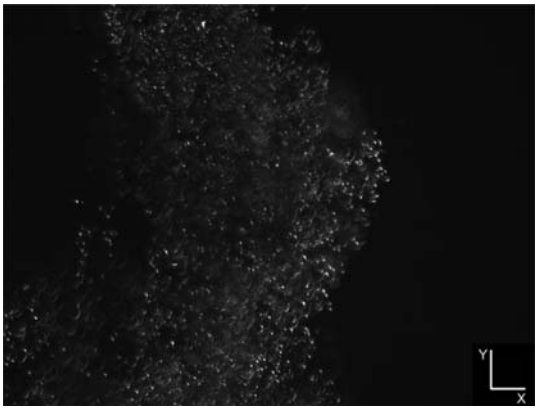

Fig. 10. Intensity distribution of the reconstructed particle field in a single plane. The meandering contour of the jet is clearly visible

5.2 Jet Flow

The holographic system was used to analyze the jet flow coming out of a syringe nozzle. This experiment was repeated 30 times on a single day. We will present one typical result. Two particle holograms were recorded with a time separation of 400 μs between the two consecutive pulses. Figure 10 shows one of the 280 unfiltered images that were captured during the reconstruction. The particles are clearly visible. Also, notice that the jet is not symmetric but has a meandering flow profile. This effect may be due to the nonideal tracer particles. After processing all the 280 images the jet's velocity profile is known. Figure 11 shows the resulting three-dimensional velocity-vector plot containing 1160 raw vectors. This vector plot shows the same meandering flow profile as was seen in Fig. 10. As expected, the main flow is in the downward $(-y)$ direction, with the highest velocities near the center of the jet. In Fig. 12 the mean downward velocity is plotted over the footprint of the jet. Again the highest velocities are found near the center of the jet.

5.3 Vortex Ring Flow

The resulting velocity field is shown in Fig. 13. The velocity field is here measured in only one plane. The main reason for this is the planar distribution of the hydrogen-bubble tracer particles. The time delay between the two recordings is 3 ms. In the correlation analysis, the transverse size of the interrogation volume is 64 pixels (= 0.4 mm), the longitudinal size is 8 pixels (= 1.6 mm) and the interrogation volume overlap is 50 %. Only the transverse component of the vectors is shown and all 1120 vectors are located in one transverse plane. A vertical vector (11 mm/s) is subtracted to compensate for the rising motion of the hydrogen bubbles.

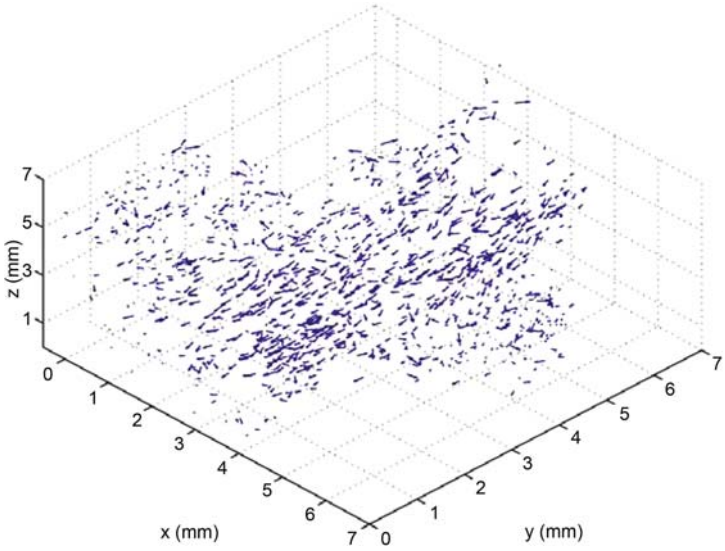

Fig. 11. Three-dimensional raw vector plot showing flow velocity inside a particle-loaded jet

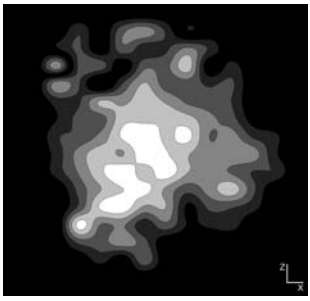

Fig. 12. Mean downward velocity over the jet's footprint. White areas correspond to a mean downward velocity of 15 cm/s

6 Future Outlook

The present system clearly demonstrates the potential of using BR films and polarization multiplexing in velocimetry measurements. As with most systems several improvements are possible. We may correct for the introduced spherical aberration in the future. As stated before, this can be achieved using an expandable water tank.

Alternative to obtaining the three-dimensional intensity distribution by scanning the reconstruction volume using the CCD camera, we will soon look into performing a single wavefront scan as described by *Barnhart* et al. [18].

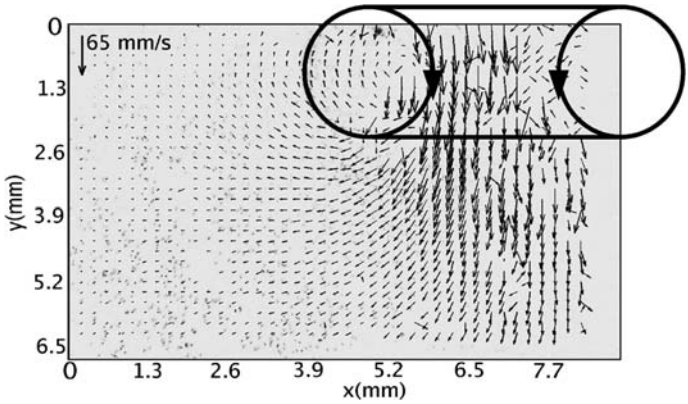

Fig. 13. Vortex-ring-flow measurement result. The illustrated plane is a slice through the center of the vortex ring

Using this digitized wavefront all particle locations may be found be digital holographic reconstruction. This method will also eliminate the inherent spherical aberration because the air–water transition can be included in the numerical model.

7 Conclusion

We have presented the first ever holographic particle image velocimetry system that uses a reusable holographic material as the recording medium. The measurement system records double-exposure holograms in a film containing the photochromic protein BR. The two constituent particle holograms are recorded in a single film using polarization multiplexing. To our best knowledge it is the first time that this type of multiplexing has been used in (particle) velocimetry measurements. The entire system delivers single pixel accuracy for more than 95 % of the generated displacement vectors.

The current system records, reconstructs, digitizes and erases a particle field hologram in less than 3 min. This allows for large-scale repetitive measurements (more than a hundred holograms on a single day), thereby enabling the acquisition of three-dimensional flow statistics. Such an experiment would be extremely laborious for a silver-halide-based HPIV system.

Although the system is still a laboratory setup, we have shown that it is possible to create an easy to operate, fully reusable HPIV camera. We believe that such a system will prove to be an extremely valuable tool for both fundamental and engineering flow study in the near future.

Acknowledgements

This work has been funded by the Foundation for Fundamental Research on Matter (FOM), the Netherlands. The authors thank Christian Poelma for his programming efforts. Furthermore, we thank Prof. Norbert Hampp (Philipps-Universität Marburg) and Donald Barnhart for their support on BR-related issues.

References

[1] C. E. Willert, M. Gharib: Digital particle image velocimetry, Exp. Fluids **10**, 181–193 (1991) 171
[2] A. K. Prasad, R. J. Adrian: Stereoscopic particle image velocimetry applied to liquid flows, Exp. Fluids **15**, 49–60 (1993) 171
[3] D. Rockwell, et al.: High image-density particle image velocimetry using laser scanning techniques, Exp. Fluids **14**, 181–192 (1993) 171
[4] D. H. Barnhart, R. J. Adrian, G. C. Papen: Phase conjugate holographic system for high resolution particle image velocimetry, Appl. Opt. **33**, 7159–7170 (1994) 171
[5] J. Zhang, B. Tao, J. Katz: Turbulent flow measurement in a square duct with hybrid holographic PIV, Exp. Fluids **23**, 373–381 (1997) 171
[6] Y. Pu, H. Meng: An advanced off-axis holographic particle image velocimetry (HPIV) system, Exp. Fluids **29**, 184–197 (2000) 171
[7] S. Herrmann, H. Hinrichs, K. D. Hinsch, C. Surmann: Coherence concepts in holographic particle image velocimetry, Exp. Fluids **29**, S108–S116 (2000) 171
[8] S. Murata, N. Yasuda: Potential of digital holography in particle measurement, Opt. Laser Technol. **32**, 567–574 (2000) 171
[9] D. H. Barnhart, N. Hampp, N. A. Halliwell, J. M. Coupland: Digital holographic velocimetry with bacteriorhodopsin (BR) for real-time recording and numeric reconstruction, in *11th Int. Symp, on Applications of Laser Techniques to Fluid Mechanics* (2002) 171
[10] N. Hampp: Bacteriorhodopsin as a photochromic retinal protein for optical memories, Chem. Rev. **100**, 1755–1776 (2000) 172
[11] N. Hampp, T. Juchem: Fringemaker – the first technical system based on bacteriorhodopsin, in A. Dér, L. Keszthelyi (Eds.): *Bioelectronic Applications of Photochromic Pigments* (IOS Press 2001) pp. 44–53 173
[12] S. D. Kakichashvili: Polarization recording of holograms, Opt. Spectrosc. (USSR) **33**, 171–173 (1972) 173
[13] L. Nikolova, T. Todorov: Diffraction efficiency and selectivity of polarization holographic recording, Opt. Acta **31**, 579–588 (1984) 174
[14] W. D. Koek, V. S. S. Chan, N. Bhattacharya, J. J. M. Braat, J. Westerweel: Polarization multiplexing based on photo-induced anisotropies in bacteriorhodopsin, in J. Coupland (Ed.): *Proc. Int. Workshop on Holographic Metrology in Fluid Mechanics* (Loughborough University Press, Loughborough 2003) pp. 123–129 174
[15] W. D. Koek, N. Bhattacharya, J. J. M. Braat, V. S. S. Chan, J. Westerweel: Holographic simultaneous readout polarization multiplexing based on photoinduced anisotropy in bacteriorhodopsin, Opt. Lett. **29**, 101–103 (2004) 174

[16] F. Liu, F. Hussain: Holographic particle velocimeter using forward scattering with filtering, Opt. Lett. **23**, 132–134 (1998) 177
[17] P. Kovesi: Phase preserving denoising of images, in *The Australian Pattern Recognition Society Conference: DICTA'99* (Australian Pattern Recognition Society 1999) pp. 212–217 180
[18] D. H. Barnhart, W. D. Koek, T. Juchem, N. Hampp, J. M. Coupland, N. A. Halliwell: Bacteriorhodopsin as a high-resolution, high-capacity buffer for digital holographic measurements, Meas. Sci. Technol. **15**, 639–646 (2004) 186

Index